

# High-heat-flux technologies for the European DEMO divertor targets: State-of-the-art and a review of the latest testing campaign

J.H. You<sup>1\*</sup>, E. Visca<sup>2</sup>, T. Barrett<sup>3</sup>, B. Böswirth<sup>1</sup>, F. Crescenzi<sup>2</sup>, F. Domptail<sup>3</sup>, G. Dose<sup>4</sup>, M. Fursdon<sup>3</sup>, F. Gallay<sup>5</sup>, H. Greuner<sup>1</sup>, K. Hunger<sup>1</sup>, A. Lukenskas<sup>3</sup>, A. v. Müller<sup>1</sup>, M. Richou<sup>5</sup>, S. Roccella<sup>2</sup>, C. Vorpahl<sup>6</sup>, K. Zhang<sup>1</sup>

<sup>1</sup>Max Planck Institute for Plasma Physics, Boltzmann Str. 2, 85748 Garching, Germany

<sup>2</sup>ENEA, Department of Fusion and Technology for Nuclear Safety and Security, via E. Fermi 45, 00044 Frascati, Italy

<sup>3</sup>CCFE, Culham Science Centre, Abingdon OX14 3DB, United Kingdom

<sup>4</sup>Università di Roma "Tor Vergata", Dipartimento di Ingegneria Industriale, Via del Politecnico 1, 00133 Rome, Italy

<sup>5</sup>CEA, IRFM, F-13108 Saint Paul Lez Durance, France

<sup>6</sup>EUROfusion, PMU PPPT, Boltzmann Str. 2, 85748 Garching, Germany

## Abstract

Divertor target is one of the most critical in-vessel components in a fusion power plant being in charge of particle and power exhaust. The targets are exposed to severe thermal loads produced by steady bombardment of impinging plasma flux. Since 2014, integrated R&D efforts have been continued aiming at developing a design concept and high-heat-flux (HHF) technologies for divertor targets of the European DEMO reactor. Recently, the second round (2017-2019) of the R&D program has been concluded. As in the first R&D round, five water-cooled target design concepts were further developed and evaluated. Fabrication technologies were improved reaching a consolidated production quality. Extensive HHF tests were conducted using small-scale mock-ups for extended loading regimes (heat flux: 20-32MW/m<sup>2</sup>). Comparative studies were performed to investigate effects of copper interlayer thickness (0.1-1mm) and different tungsten armour materials. In the present paper, the final results of the second round HHF testing campaign are reported. The HHF performance of each design variant is discussed based on in-situ diagnostic data (infrared thermography), ultrasonic inspection images and post-mortem metallographic micrographs. All monoblock-type design concepts passed the specified qualification criterion ( $\geq 500$  pulses at 20MW/m<sup>2</sup>, coolant: 130°C) without any failure or armour cracking. Moreover, two of them (ITER-like and composite pipe) remained fully intact even under 25MW/m<sup>2</sup> (100 pulses) and 32MW/m<sup>2</sup> (5 pulses).

Key words: Fusion reactor, DEMO, Divertor, Vertical target, High heat flux, Tungsten monoblock

\*Corresponding author: Jeong-Ha You (you@ipp.mpg.de)

## 1. Introduction

Divertor target of a nuclear fusion reactor is a key in-vessel component having critical operational functions to exhaust particles (helium ash and impurity) and associated thermal power [1]. For this, divertor targets shall be exposed to intense plasma bombardment and severe heat fluxes on the surface. The maximum heat flux peaking at the strike point is expected to reach 10MW/m<sup>2</sup> during a long-pulse (2h) normal operation and up to 20-40MW/m<sup>2</sup> in slow transient events (1-10s) [2-4]. The most acute thermal loading case is edge localized modes ( $\leq 1\text{MJ/m}^2$ ,  $\leq 1\text{ms}$ ) whereas the heaviest loading situation is central disruption ( $\sim 1\text{GJ/m}^2$ ,  $\sim 10\text{ms}$ ) in a fusion power reactor such as DEMO [5], where damage of armor (tungsten) surface is likely to occur [6]. Furthermore, in DEMO, the materials of divertor targets will experience embrittlement due to neutron irradiation [7-11]. The end-of-life damage dose in the DEMO

divertor target is predicted to reach 1.5-3 dpa for the tungsten armor and 6-13 dpa for the copper pipe. These damage doses are one order of magnitude higher than the ITER case [7, 8]. Coolant pressure (50 bar), thermal stresses (several 100MPa) and electromagnetic impact forces ( $\sim 1\text{MN}$ ) pose substantial mechanical loads [12-14].

Reliability and longevity of divertor targets compatible with the harsh and complex loading environment of a fusion power plant is the most crucial engineering requirement for assuring power exhaust and thermal management. The major challenge is to develop high-heat-flux (HHF) technologies with a high technology readiness level [15]. Currently, it remains an open question what types of operational scenarios have to be taken into account as mandatory load cases in the load specifications. Severe off-normal events such as disruptions may need to be considered as rare but possible load cases because it will be

very difficult to fully avoid such events and the design shall ensure structural resilience against the accidental impact loads for a few times. However, massive melting of the armor will probably hardly allow continued use of the affected plasma-facing component if the damage due to melting is excessive. On the contrary, the load cases for normal operation should be specified as far as possible because they set the guidelines as minimum requirements for design, technology and validation. The question is what loading scenarios should be included in the definition of the normal operation regime in addition to the stationary flat top phase. Should the loss of detachment be regarded as an inevitable instance of normal operation, targets will have to withstand a limited number of slow transients (20-25MW/m<sup>2</sup>) over the whole lifetime. At present, it seems difficult to identify the complete spectrum of slow transients for the DEMO given the complexity of the physics of plasma instability (e.g. L-H transition). Thus, the intensity (heat flux) and pulse duration of slow transients are not confirmed yet. In the present study, a pragmatic design target was defined for engineering purpose in such a way that the maximum possible HHF load achieved by the best current technology was taken as the qualification criterion for normal operation.

In the framework of the EUROfusion Consortium since 2014, an integrated multidisciplinary R&D efforts were conducted to develop and to verify design concepts and technologies of the divertor target for the European DEMO [16]. In the work package ‘Divertor’ (WPDIV), preconceptual design studies and technology R&D tasks including HHF qualification tests were performed. Multiple design concepts incorporated with innovative technology options were handled. The present paper presents the major results of the latest HHF test campaign performed for the small-scale target mock-ups developed in the 2nd R&D phase of WPDIV (2017-2019).

## 2. Target design concepts and test mock-ups

As in the first R&D phase [16], likewise in the second phase the five water-cooled target designs were further developed, where four of them were based on a tungsten mono-block type with a copper-base cooling pipe while the other had the form of tungsten flat tile type joined on a copper composite cooling block. The essential design features were as follows:

- W mono-block joined with a CuCrZr cooling pipe and a Cu interlayer (“ITER-like”)
- W mono-block joined with a CuCrZr cooling pipe and a Cu thermal break interlayer (“Thermal break”)
- W mono-block with a W wire-reinforced Cu composite pipe (“Composite pipe”)
- W mono-block joined with a thin (20μm) or thick (500μm) functionally graded W/Cu interlayer (“FGM interlayer”)
- W flat tiles with a W particle-reinforced Cu composite heat sink block (“Composite block”)

Fig. 1 shows the characteristic design features of the DEMO divertor target concepts. For the details of design rationales [16, 17], design studies [18-21] and technology progress [22-25] achieved in the second R&D phase, readers are referred to the given references.

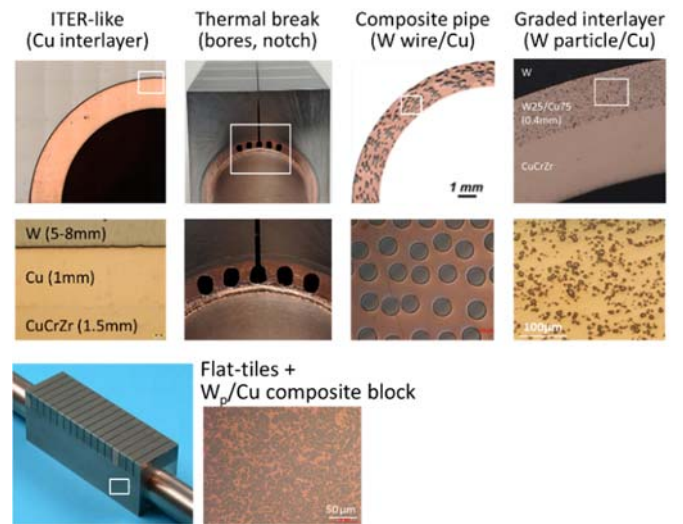


Fig. 1. Characteristic design features of the DEMO divertor target concepts developed in the pre-conceptual R&D phase of the EUROfusion program.

For the sake of completeness, the underlying design logics of the selected target design concepts are briefly described again in what follows. The materials of the constituents and the key design logics are summarized in Table 1.

Table 1. A brief description of the target design concepts.

| Target concepts              | Interlayer       | Heat sink                | Design logics                               |
|------------------------------|------------------|--------------------------|---|
| ITER-like (W monoblock)      | Cu (1mm)         | CuCrZr pipe              | baseline (reduced width), prevent cracking  |
| Thermal break (W monoblock)  | Cu (1.5mm) bores | CuCrZr pipe              | mitigate heat flux peaking, reduce stress   |
| Composite pipe (W monoblock) | None             | W <sub>p</sub> /Cu pipe  | enhance strength of the pipe, reduce stress |
| FGM interlayer (W monoblock) | W/Cu (0.5mm)     | CuCrZr pipe              | reduce stress, improve bonding              |
| Composite block (W tiles)    | None             | W <sub>p</sub> /Cu block | maximize design margin of the heat sink     |

The ITER-like design was taken as the baseline because this design has been extensively tested in the ITER R&D program and proved to be suitable for the ITER-relevant HHF loads. The only difference between the original ITER target design and the present model is the cross section width of the monoblock (28mm vs. 23mm). The reason for the reduced section width is to reduce the stress intensity (driving force for crack initiation) on the armor surface so that the maximum possible crack size is limited below 2mm if there is any fatigue crack formed on the surface [13, 16].

The thermal break design is based on the idea that the margin to the critical heat flux (onset of film boiling) can be increased by reducing the heat flux concentration on the upper area of the pipe perimeter. To this end, axial bores are introduced into the copper interlayer as shown in Fig. 1. The bores impede the thermal conduction so that the heat flow bypasses the top area mitigating the heat flux peaking while fully utilizing the larger area of the pipe perimeter for heat transfer. At the same time, thermal stress in the pipe is reduced as well.

The composite pipe design is a cognate variant of the ITER-like baseline where the copper alloy cooling pipe is replaced

by the W wire-reinforced Cu composite pipe to enhance the strength of the pipe under cumulative slow transient loads. A critical concern regarding the use of precipitation-hardened CuCrZr alloy as structural material is the issue of irreversible softening under long-term thermal exposure at temperatures above 350°C due to microstructural ageing (Ostwald ripening of the precipitates) and irradiation creep. On the contrary, the composite pipe does not undergo thermal softening owing to the excellent thermal stability of the refractory reinforcement even at high temperatures above 1000°C [26, 27].

The aim of the FGM interlayer design is either to reduce stress (thick FGM layer) by a graded interlayer reducing the thermal expansion (or contraction) mismatch or to improve bonding (thin layer) by a graded composition profile. The motivation to test the thin interlayer design was to explore the feasibility of excluding the thick copper layer. The reason of this idea is the experimental finding that pure copper tends to be fully embrittled under fast neutron irradiation at around 350-400°C due to the grain boundary segregation of transmuted helium bubbles [28].

The composite block design was motivated by the potential need to increase the design margin of the heat sink against the structural failure criteria. This design will have advantage in the case when the heat sink (CuCrZr alloy) is subject to failure risk due to exhausted ductility under neutron irradiation [29]. The massive heat sink block (replacing the copper alloy pipe and the tungsten block) offers much greater resilience against brittle failure owing to the large volume. Fatigue fracture life will be increased because larger cracks can be tolerated in the heat sink block compared to the pipe geometry. Moreover, the use of the W/Cu composite enhances strength [30-32].

The mock-ups of the second phase had a similar geometry as the first phase but the dimensions were slightly modified. The armor thickness (distance from the interlayer to the top face) was increased from 5mm to 8mm to enhance erosion lifetime. The axial thickness of the blocks was increased from 4mm to 12mm to reduce manufacturing costs (see Fig. 2).

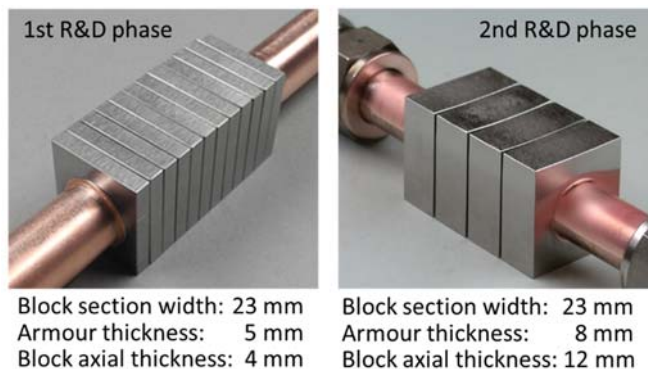


Fig. 2. Monoblock-type small-scale test mock-ups of divertor target fabricated and tested in the first (left) and the second (right) R&D phase, respectively.

In the second phase, there were several technical evolutions as follows:

- FGM interlayer: 20 $\mu$ m (PVD) vs. 500 $\mu$ m (cold-spray) [24]
- Thermal break: spoke vs. circular bore [20]
- Composite pipe: 150 $\mu$ m wire vs. 50 $\mu$ m wire [25]

For FGM, cold spray method was used for fabrication of the thick coating because the deposition rate of PVD (magnetron sputtering) is too low to be practicable for producing a thick coating.

For the thermal break, the spoke type geometry was replaced by circular bores to avoid rupture of the thin spokes due to plastic strain concentration.

For composite pipe, thinner wires were used for braiding as they show much higher tensile strength than thicker wires.

Two different commercial products of tungsten were used for the armour blocks for a comparative evaluation, namely, from the Japanese company ALMT and Chinese company AT&M. A commercial CuCrZr alloy (ELBRODUR) delivered from the company KME was used for the cooling pipe.

Small-scale test mock-ups were manufactured for the HHF tests (see the proxy in Fig. 2 right). The key step of mock-up fabrication was joining. The applied joining methods were:

- ITER-like (ALMT): Hot radial pressing (HRP)
- ITER-like (AT&M): Hot radial pressing (HRP)
- Thermal break: Brazing
- Composite pipe: Brazing
- FGM interlayer (thick): Hot isostatic pressing (HIP)
- Composite block: Casting (infiltration)

The selection of these joining technologies was an outcome of empirical trials considering the given laboratory infrastructure and industry partnership.

### 3. HHF test condition

The HHF test campaign of the second phase comprised two sets of test program: fatigue test (at 20MW/m<sup>2</sup>) and overload test (at 25MW/m<sup>2</sup>). In both test programs a screening test (for detecting faults) was carried out for individual mock-ups prior to the main test.

The sequence of the fatigue test procedure was as follows:

- 1) 1st screening test (cold water: 20°C, 1MPa, 12m/s): stepwise loading from 6 to 25MW/m<sup>2</sup>, 5 pulses
- 2) 2nd screening test (cold water: 20°C, 1MPa, 12m/s): cyclic loading at 10MW/m<sup>2</sup>, 100 pulses
- 3) 3rd screening test (hot water: 130°C, 4MPa, 16m/s): stepwise loading from 6 to 25MW/m<sup>2</sup>, 5 pulses
- 4) Pre-test (hot water: 130°C, 4MPa, 16m/s): cyclic loading at 20MW/m<sup>2</sup>, 100 pulses
- 5) Main test (hot water: 130°C, 4MPa, 16m/s): cyclic loading at 20MW/m<sup>2</sup>, 500 (or 1000) pulses

The sequence of the overload test procedure was as follows:

- 1) - 2): identical to the step (1) and (2) of the fatigue tests
- 3) 3rd screening test (cold water: 20°C, 1MPa, 12m/s): stepwise loading from 6 to 32MW/m<sup>2</sup>, 5 pulses
- 4) Main test (cold water: 20°C, 1MPa, 12m/s): cyclic loading at 25MW/m<sup>2</sup>, 100 (or 200) pulses

A new mock-up was used for each fatigue test or overload test. The cooling condition for the fatigue test was approximately adapted to the actual cooling condition of the DEMO divertor whereas cold water was used for the overload test to maintain sub-cooled boiling regime.

The HHF tests were carried out at the hydrogen neutral beam

facility GLADIS (Max Planck Institute for Plasma Physics). The technical data of the facility and the issues related to the diagnostic instruments are described in detail in [33, 34]. The length of each heat pulse time was set at 10s to ensure thermal equilibrium in the mock-ups. The beam diameter was 70mm at the target position.

Surface temperature of the armor blocks was measured using one-color (spot: 22mm, temp.: 350°C-3500°C) and two-color (8mm, 500°C-1700°C) pyrometer. Infrared (IR) camera was used to monitor the temperature evolution from pulse to pulse. Based on the calorimetric calibration, a constant emissivity value of 0.3 was assumed for the one-color pyrometer data (error range:  $\pm 5\%$ ). The net absorbed thermal power showed a linear proportionality with the surface temperature up to 32MW/m<sup>2</sup> confirming an intact structural integrity and good fabrication quality [34]. The beam power fluctuation between pulses remained within  $\pm 5\%$ .

Fig. 3 illustrates the calculated temperature distribution in the tungsten block (left) and the cooling pipe (right) of the ITER-like target mock-up (2<sup>nd</sup> phase) during the thermal equilibrium at 20MW/m<sup>2</sup> (coolant: 150°C). The discrepancy between the measured and the calculated maximum armour temperature was about 10% (2000-2100°C vs. 2260°C). In the cooling pipe, the maximum temperature reached about 430°C.

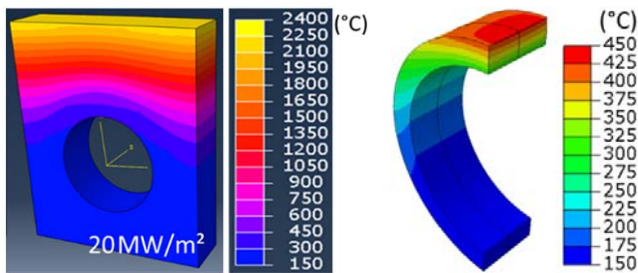


Fig. 3. Calculated temperature distribution in the tungsten block (left) and the cooling pipe (right) of the ITER-like target design (armour: 8mm) at 20MW/m<sup>2</sup> (coolant: 150°C).

## 4. Results of the HHF fatigue tests (20MW/m<sup>2</sup>)

### 4.1. HHF performance of different design concepts

All mock-ups of the monoblock-type target designs survived at least 500 pulses of 20MW/m<sup>2</sup> heat flux without undergoing any macroscopic failure. The mock-ups of the composite pipe design and the FGM interlayer design withstood even 1000 pulses without failure. The corresponding IR camera images are shown in Fig. 4 where the surface temperature distribution of each mock-up during the thermal equilibrium at the first and the 500th pulse is compared. Note that the weak heterogeneity of the color shade found at the 500th pulse is not a real effect, but an artefact caused by local emissivity change due to the evolving surface roughness. However, the change of the color shade (thus temperature) seems negligible. This indicates that all mock-ups remained intact without discernable structural failure. These results are comparable to those of the first phase HHF test campaign where also all monoblock-type mock-ups had successfully passed the same test condition as well. [16]

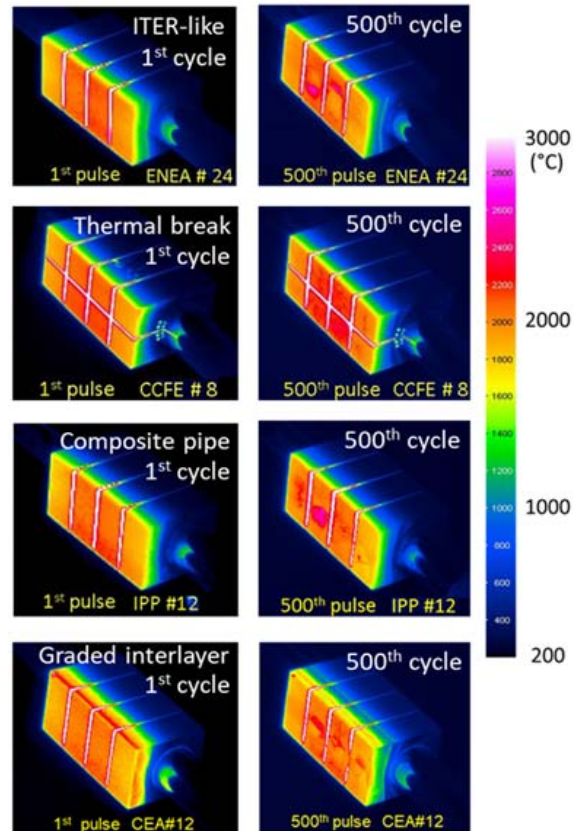


Fig. 4. IR camera images of the monoblock-type target mock-ups of four different design variants (armour: 8mm) tested at 20MW/m<sup>2</sup> using hot coolant water (130°C). Armour surface temperatures at the 1st (left) and at the 500<sup>th</sup> (right) pulses are compared (the color scale of temperature is only indicative).

Fig. 5 shows the photographs of the surface of the same tested mock-ups. Extensive surface roughening formed by inelastic deformation was observed. The maximum height measured by a laser profilometer was  $\sim 70\mu\text{m}$ . Otherwise, no crack (on a microscopic scale down to a few 10 $\mu\text{m}$ ) was found.

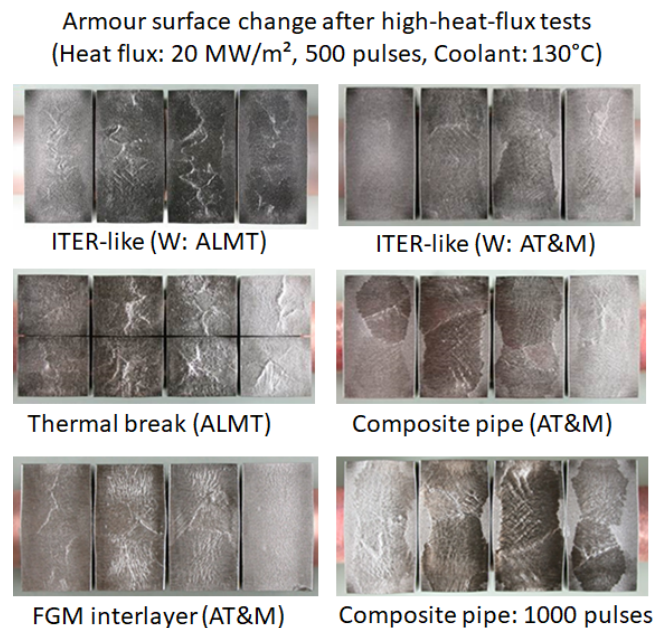


Fig. 5. Photographs of the monoblock-type target mock-ups of four design variants tested at 20MW/m<sup>2</sup> up to 500 pulses.

Fig. 6 shows a metallographic image of the longitudinal cut section of the ITER-like design mock-up (W armour: ALMT) after the HHF test (500 pulses). Microscopic scrutiny revealed no evidence of significant damage or failure. The both joining interfaces (W armor/Cu interlayer and Cu interlayer/CuCrZr cooling pipe) remained obviously intact. The upper part of the armour showed homogeneous volumetric swelling (typically a few volume %). The swelling was generally found in all mock-ups tested at 20MW/m<sup>2</sup>. A FEM study indicated that the swelling was possibly caused by inelastic strains (plastic flow, creep) [19]. Note that the plastic deformation of the pipe wall was due to the applied pressure during fabrication (HRP).

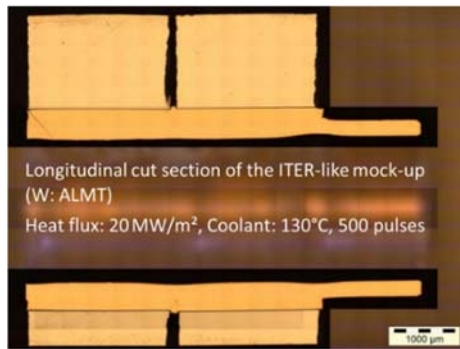


Fig. 6. Metallographic image of the longitudinal cut section of the ITER-like design mock-up (W armour: ALMT) after the HHF test (20MW/m<sup>2</sup>, 500 pulses).

Fig. 7 shows a detailed metallographic view of the same cut section (left block) as in Fig. 6 with the superposed EBSD (Electron Back-Scatter Diffraction) scan maps measured on the selected regions. The EBSD examination showed that the armour region above the temperature level of 1200°C (4.8mm from the top face) was mostly recrystallized as expected [33]. Surprisingly, the EBSD maps (and micrographs) revealed that the uppermost layer (up to 1mm at the middle) underwent an abnormal grain growth leaving only a few large grains with a large-angle grain boundary. It is remarkable to note that even such very coarse and fully recrystallized (i.e. softened) grains did not lead to a formation of any low cycle fatigue crack. This positive feature can be attributed to the weakened stress effect realized by the reduced block width dimension (23mm instead of 28mm) as was predicted by dedicated fracture-mechanics studies [13, 18]. This remarkable result was representative for all other monoblock-type mock-ups tested here.

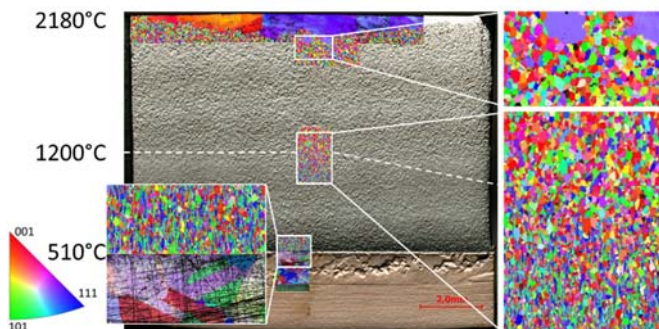


Fig. 7. A longitudinal cut section of the ITER-like mock-up made of ALMT tungsten blocks after the HHF fatigue test at 20MW/m<sup>2</sup> (500 pulses). The heat-loaded part of two blocks are shown (the same as in Fig. 6) together with EBSD maps.

Fig. 8 shows the longitudinal cut sections of all monoblock-type mock-ups of different design variants after the HHF tests (500 pulses). As in the case of the ITER-like design (Fig. 6), the mock-ups of all other design variants remained fully intact without any notable damages or failure (the thin gaps seen in the thermal break interlayer are not defects but bores).

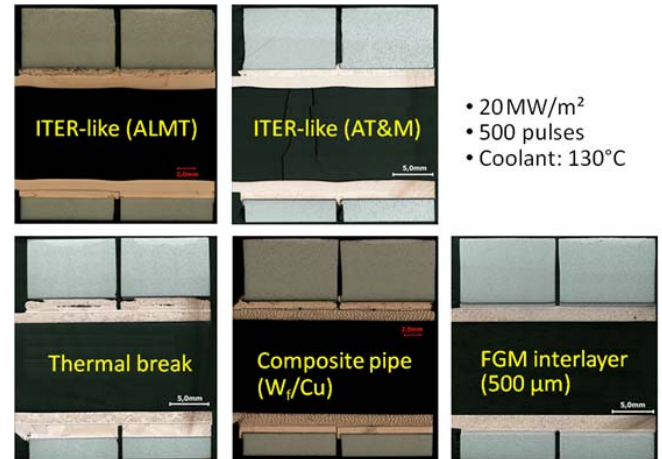


Fig. 8. Metallographic images of the longitudinal cut sections of all monoblock-type mock-ups of different design variants after the HHF tests (20MW/m<sup>2</sup>, 500 pulses). Different colors were due to the different light reflection under the microscope.

Fig. 9 and 10 show the in-situ diagnostic images of the mock-up of the composite block design. Shown are an IR image and a CCD camera image during the screening test (5 pulses) at 25MW/m<sup>2</sup> (Fig. 9) and CCD camera images during the HHF fatigue test at 20MW/m<sup>2</sup> (1<sup>st</sup> pulse and 200th pulse) (Fig. 10). An optical micrograph of the lateral face after the test is also shown (Fig. 10). The screening test showed that the composite block design had a thermal capacity at least up to 25MW/m<sup>2</sup> (the mock-up remained intact for 5 cycles). The failure of the left edge tile was due to a fabrication fault. In the fatigue test at 20MW/m<sup>2</sup>, overall failure occurred at the 167th pulse. The composite block design failed the fatigue test at 20MW/m<sup>2</sup>. The microscopic image reveals that the failure was due to the detachment of the tungsten tiles from the composite block. The detachment seems to have been initiated by cracking at the free surface edge of the interface where a singular stress concentration prevails [35, 36]. In the course of cyclic pulses, the crack extends further inwards either by cumulative plastic fatigue of the thin Cu layer (~50µm) aggravated by thermal softening at high temperature (~700°C) or by brittle fracture of the armor.

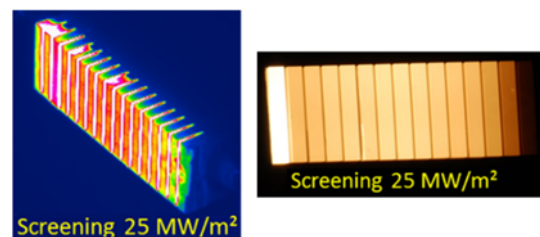


Fig. 9. IR picture (left) and CCD camera image (right) of the mock-up of the composite block design during the screening test at 25MW/m<sup>2</sup> (5 pulses).

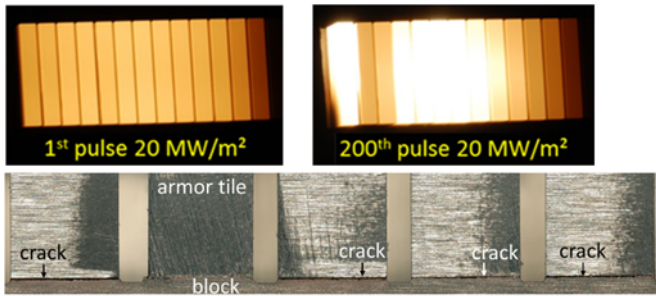


Fig. 10. CCD camera image of the mock-up of the composite block design during the fatigue test at  $20\text{MW/m}^2$  (upper left: 1st pulse, right: 200th pulse) and optical microscope image of the lateral face after the test (below).

#### 4.2. Comparison between two different tungsten materials

Fig. 11 shows the IR and CCD camera images of two ITER-like design mock-ups, each with the AT&M (left) and ALMT (right) tungsten blocks respectively. Compared are the states at the first and the final (500th) pulse of  $20\text{MW/m}^2$  load. The slight difference in the color shade between the two loading stages was due to the changing emissivity caused by surface roughening and had nothing to do with real defect. No distinct hot spot was seen indicating an intact joint integrity. The postmortem metallographic section images in Fig. 11 also confirmed that both mock-ups indeed remained intact and no critical material damage was found. A minor difference is seen that the depth of the large grains near the surface of the ALMT tungsten was slightly larger than that of the AT&M tungsten. However, this finding had a limited statistical significance due to the small number of section images available.

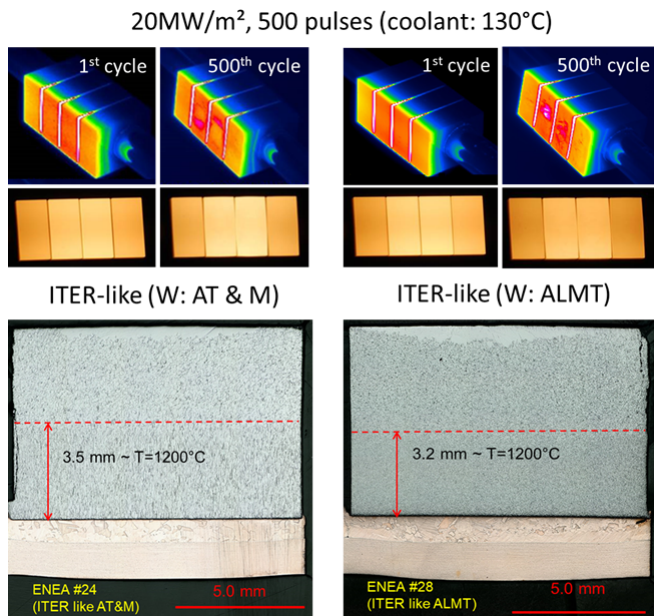


Fig. 11. IR/CCD camera images and metallographic section views of two ITER-like design mock-ups, each with AT&M (left) and ALMT (right) tungsten blocks. Compared are the first and the 500th pulse at  $20\text{MW/m}^2$ .

For making an examination of overall state of joint integrity, ultrasonic inspection was applied along the joining interface. The test revealed that the ITER-like mock-up with the AT&M tungsten blocks experienced a localized debonding at the free

edge of the bond interface between the Cu interlayer and the CuCrZr pipe whereas the mock-up with the ALMT tungsten blocks remained fully intact (see Fig. 12). A similar damage feature has already been observed in the first phase ITER-like mock-up [37]. Previous fracture mechanics studies elucidated the theoretical cause of a preferred crack initiation at the free surface edge of a bond interface between dissimilar materials under HHF loads [38, 39].

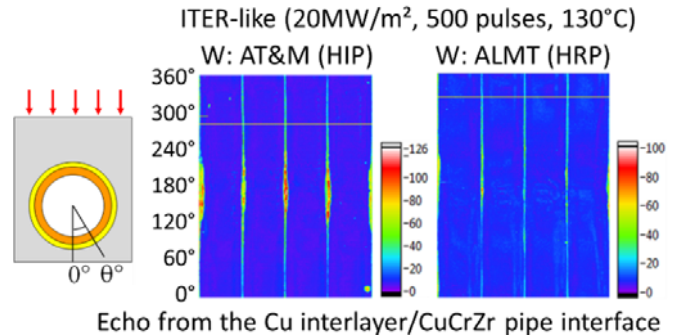


Fig. 12. Ultrasonic inspection results depicting the reflected echo signal profiles (C-scan) detected from the bond interface between the Cu interlayer and the CuCrZr pipe. Compared are two ITER-like mock-ups each with the AT&M (left) and the ALMT (right) tungsten blocks. The thin hot spots with higher signal intensities indicate potential defect sites.

#### 4.3. Effect of copper interlayer thickness

Fig. 13 shows IR/CCD camera images (left) of the mock-ups of the two ITER-like design variants each with a 0.1mm or 0.3mm thick copper interlayer. Photographs of the armour top surface (AT&M tungsten) after the tests are also shown (right). Note that the white spot on the IR image of the 0.1mm Cu interlayer case is an artefact by locally changed emissivity due to surface roughening (coincides with the surface topography). On the contrary, the reddish hot spots occurring near the free edges of the gaps were real effects due to defect formation as confirmed by the ultrasonic examination (see Fig. 14).

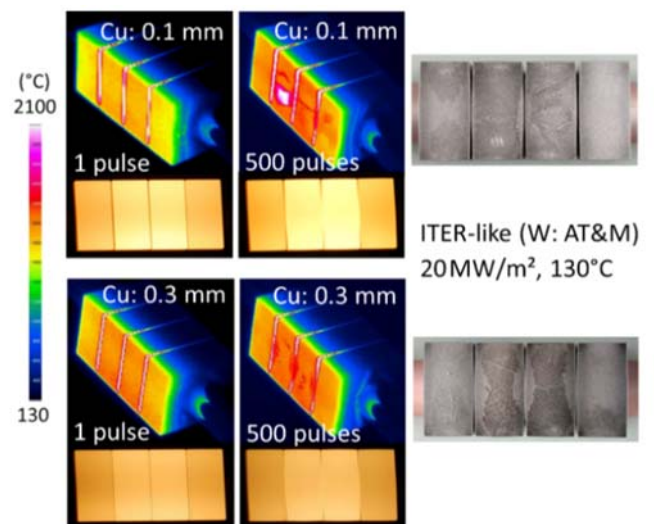


Fig. 13. IR/CCD camera images at the first and the 500th pulse of two ITER-like design mock-ups each with a 0.1mm and 0.3mm thick copper interlayer. Photographs of the armour (AT&M tungsten) surface after the tests are also shown (right).

Fig. 14 shows the ultrasonic echo signal profiles (C-scan) of three variants of the ITER-like mock-ups after the HHF tests, each with a 0.1mm, 0.3mm and 1mm thick Cu interlayer. The echo was reflected from the bond interface between the Cu interlayer and the CuCrZr pipe. The C-scan image of the same mock-ups before HHF testing showed no damage (not shown here) [40]. This means that the damage features found in Fig. 13 are results of the HHF loads.

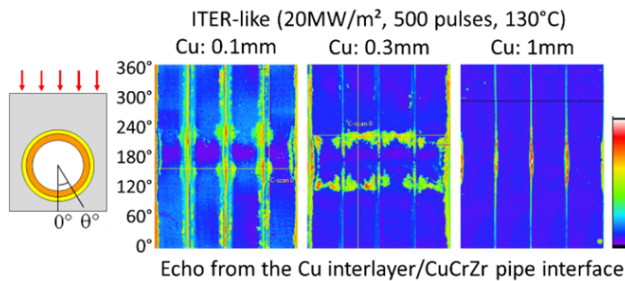


Fig. 14. Ultrasonic C-scan profiles of three variants of the ITER-like design mock-ups each with a 0.1mm, 0.3mm and 1mm Cu interlayer (echo from the interlayer/pipe interface).

The C-scan of the 0.1mm interlayer case clearly exhibits local debonding along the entire free edge of the Cu/CuCrZr bond interface with larger damaged areas on the heat-loaded side (particularly at angular positions of 150° and 210°). The C-scan of the 0.3mm interlayer case reveals a pronounced failure pattern along two specific angular positions (where the hoop stress becomes maximum) on the heat-loaded side. Free edge debonding is rarely seen. From this result, it can be concluded that a thicker Cu interlayer ( $>0.3\text{mm}$ ) is beneficial from the structural integrity point of view. 1mm seems to be an optimal thickness to ensure a sufficient amount of plastic dissipation in the ductile layer relaxing the stored strain energy and thus reducing the driving force for crack initiation (as predicted by the FEM-based design optimization study [41]).

## 5. Results of the overload tests (25-32MW/m<sup>2</sup>)

### 5.1. HHF performance of different design concepts

The mock-ups of the ITER-like, thermal break and composite pipe design survived the screening test at 32MW/m<sup>2</sup> (thermal break design: up to 30MW/m<sup>2</sup>) and the subsequent overload test at 25MW/m<sup>2</sup> ( $\geq 100$  pulses) without any discernable crack formation in the armor or structural failure of the joints (see Fig. 15). Three identical mock-ups of the ITER-like design were tested at the overload and all of them successfully passed the test indicating a reliable production quality. Minor damage (roughness) of the armor surface is found on all monoblocks. The FGM mock-up with the thin interlayer failed the overload test. The FGM mock-up with the thick interlayer partially (1-2 blocks) failed the overload test.

The mock-up of the thermal break design survived screening test up to 30MW/m<sup>2</sup> (30 pulses) without cracking (also on a microscopic scale) or armor melting. However, it underwent global melting of the armor surface at 32MW/m<sup>2</sup> (see Fig. 16) [34]. The depth of the melt layer was roughly 3mm. In the solidified layer, only a few large grains were formed in the vertical direction. Even in the circumstance of massive armor melting, the joint itself remained intact.

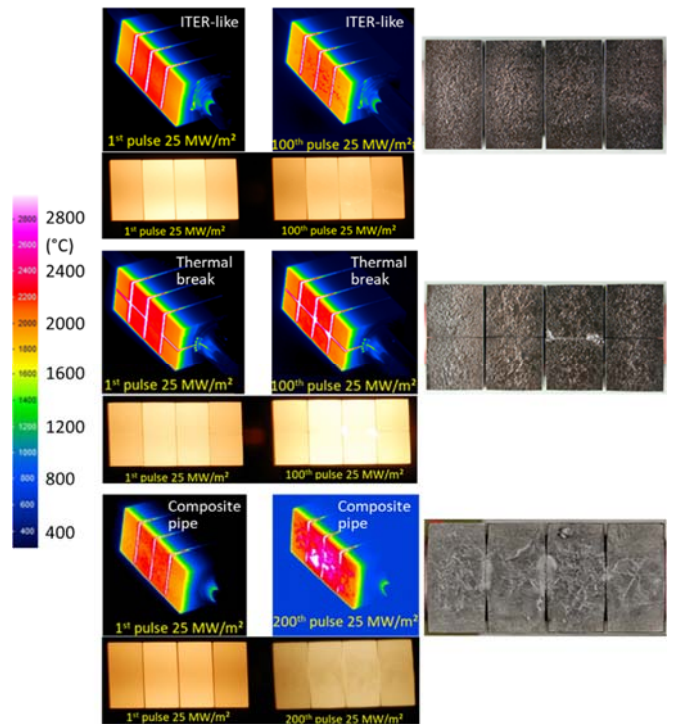


Fig. 15. IR/CCD camera images of the mock-ups at 25MW/m<sup>2</sup> (1st vs.100th pulse) of the ITER-like (top), the thermal break (middle) and the composite pipe design (bottom, 200th pulse). The photographs (right) of the armor surface show the damage (roughening) caused by plastic deformation.

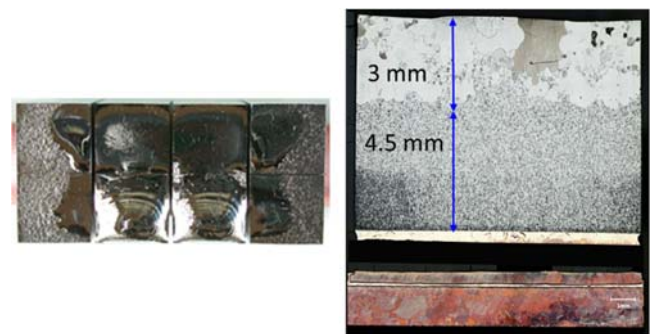


Fig. 16. Photograph of the armor top surface (left) and optical microscopic image of the metallographic cut section (right) of the thermal break mock-up after a screening test at 32MW/m<sup>2</sup>.

### 5.2. Comparison between two different tungsten materials

The mock-ups of the ITER-like design (Cu interlayer: 1mm) fabricated with the AT&M as well as ALMT tungsten blocks fully survived the overload tests. Fig. 17 shows an IR image at 32MW/m<sup>2</sup> and the CCD camera image at 25MW/m<sup>2</sup> (100th pulse). No distinct hot spot is seen. The average temperature of the two middle blocks was slightly higher compared to the both side blocks. This effect was owing to the characteristic Gaussian distribution of the beam power density [42]. The relatively homogeneous surface temperature distribution was deemed an evidence that the mock-ups were intact without failure. The photographs of the armour top surface clearly manifest that no visible crack was produced. Only a modest roughening (several 10 $\mu\text{m}$ ) was observed.

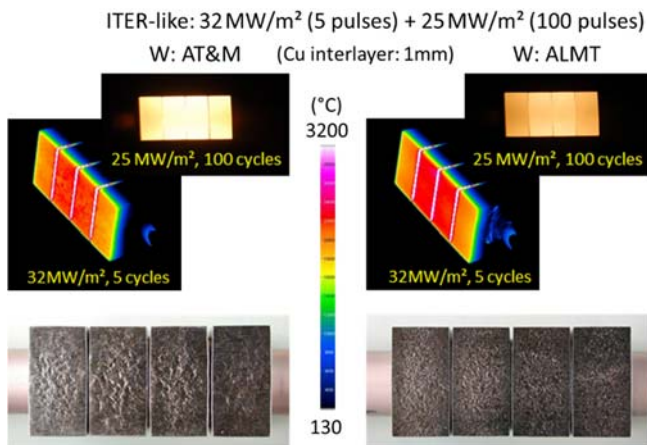


Fig. 17. IR/CCD camera images respectively at 32MW/m<sup>2</sup> (5th pulse) and at 25MW/m<sup>2</sup> (100th pulse) of two ITER-like design mock-ups each made of AT&M and ALMT tungsten blocks, respectively.

### 5.3. Effect of copper interlayer thickness

The mock-ups of two ITER-like design variants each with a 0.1mm or 0.3mm thick Cu interlayer passed the overload tests as well without any global failure as demonstrated in Fig. 18. Ultrasonic inspection has not been made yet for these mock-ups, thus for the moment, no definite statement about damage features can be given. A further extension of loading cycles is considered to accumulate fatigue damage.

It is remarkable that all monoblock-type mock-ups performed with excellent robustness and reliability for such an extensive range of HHF loads as considered here. There was a concern with regard to the trend of deep crack formation at the armour surface of a tungsten monoblock-type target when subjected to a fatigue load (>300 pulses) at around 20MW/m<sup>2</sup> [43, 44]. The deep cracking mechanism was clarified in [45] and the effect of dimension was elucidated in [18]. The present study delivers an experimental evidence for these interpretations.

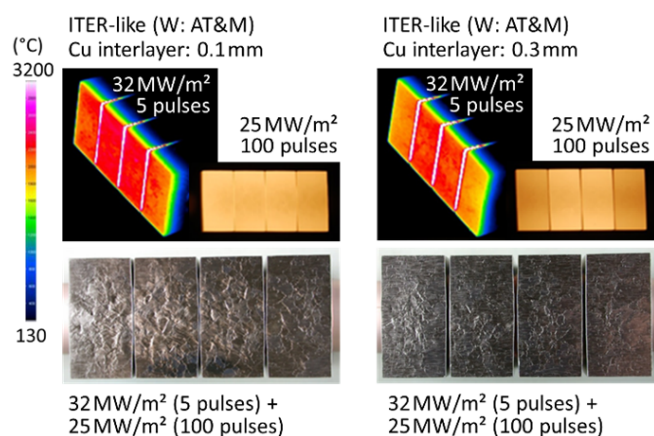


Fig. 18. IR/CCD camera images respectively at 32MW/m<sup>2</sup> (5th pulse) and at 25MW/m<sup>2</sup> (100th pulse) of two ITER-like design mock-ups (0.1mm vs. 0.3mm thick Cu interlayer).

## 6. Implications for future research

The present HHF test results give us far reaching implications in view of R&D strategy and testing program. In the following

selected issues are addressed focusing on the material aspect.

### 6.1. Material issues for tungsten armor

One of the most pronounced findings from these HHF tests is the fact that the tungsten armor of all mock-ups survived the entire fatigue (20MW/m<sup>2</sup>) or overload (25MW/m<sup>2</sup>) test cycles without forming any discernible cracks even though the upper half of the armor has been fully recrystallized and the surface layer has undergone abnormal grain growth. It is noted that this positive result is attributed to the reduced dimension of the monoblock section width. This means that if the reduced block width is accepted for the design of the DEMO divertor, metallurgical efforts to improve the microstructural resistance against recrystallization may not be necessary anymore. This statement may still be valid even under neutron irradiation as the lattice damage will be mostly recovered around the surface temperature range at the strike-point. Once recrystallization is accepted, a much wider operational regime will be available for the designers (the 1200°C temperature limit will not be applicable for normal operation).

It should be noted that the present results represent only HHF performance without potential effect of combined loads (e.g. neutron irradiation, mechanical constraint). The question as to whether these results can be extrapolated to the real operation condition remains open. A recent FEM study showed that the tungsten monoblocks of the ITER-like target would remain intact without critical cracking at least up to 20MW/m<sup>2</sup> even in a fully embrittled state with a reduced tensile strength [46]. The findings of both the HHF tests and the FEM prediction indicates that the currently available commercial products of tungsten will have a highly promising chance to be qualified for a higher TRL (Technology Readiness Level) including the nuclear operational condition of DEMO. It is noted that the recrystallization per se will only have negligible effects on the atomic sputtering and tritium retention behavior [47].

### 6.2. Material issues for joint

Metallographic preparation and microscopic analysis of the tested mock-ups are currently ongoing for direct examination of damage or potential failure in the bond interface region. It is noted that the in-situ diagnostics and the post-test ultrasonic inspection showed that the joints of all mock-ups remained mostly intact in both the fatigue and overload tests (except the mock-ups with the thin copper interlayer). This indicates that the current joining technology satisfies the ITER qualification criterion and has reached the physical limit (melting of armor).

The next milestone towards qualification for DEMO would be neutron irradiation and post-irradiation HHF tests in a hot cell. This test is an indispensable step for the technology validation prior to the Engineering Design Phase since only an empirical test can allow ultimate qualification of the joints in terms of fatigue performance under nuclear environment. To this end, a dedicated irradiation and post-irradiation HHF test program is under planning in the framework of the Eurofusion program.

### 6.3. Further HHF testing programs: outlook

The HHF test program conducted so far was focused on the thermal fatigue performance of joints and armor. In DEMO, the flat top pulse duration will reach up to 2 hours. Under such a long-term thermal exposure, viscous effects and irreversible

ageing of the materials may occur at the strike point region if peak heat flux density approaches 20MW/m<sup>2</sup> in the normal operation. In this circumstance, the Cu interlayer can possibly experience premature rupture due to creep-fatigue interaction leading to a global failure of the component. The creep-fatigue interaction will not be a significant effect for the CuCrZr pipe since the stress state of the pipe is expected to remain mostly within the elastic regime owing to elastic shakedown provided that softening by ageing is not significant [48]. To address this issue, a long-pulse (600s) HHF (20MW/m<sup>2</sup>) test is currently carried out for the ITER-like design mock-ups in 2020 at an electron beam facility (HELICZA).

Another testing program in preparation is short-pulse ( $\leq 0.5s$ ) overload (40MW/m<sup>2</sup>) test to be carried out in 2020-2021. This testing mode is to simulate the strike-point sweeping scenario which is considered for DEMO as an option for mitigating the heat flux in the event of plasma reattachment [49, 50]. One of the testing objectives is to explore the thermal loading limit of the armor in an intermediate pulse length range where the heat wave propagates in a transient mode giving thermal impact to the main volume of the armor.

#### 6.4. Down-selection of target design concepts

Based on the present HHF test results, a decision was taken to select a target design eligible for the subsequent conceptual design phase. The ITER-like design (together with the joining technology) was confirmed again as the baseline because the mock-ups of this design passed the qualification tests with the best record (together with the mock-ups of the composite pipe design). In addition, the composite pipe design was selected as a back-up option. As mentioned earlier, the composite pipe design is a cognate variant of the ITER-like design, thus it is not regarded as an independent alternative design, but rather an advanced technology option.

## 7. Summary and conclusions

All HHF test results from the 2nd preconceptual R&D phase of WPDIV for DEMO divertor target are summarized in Table 2. All monoblock-type water-cooled design concepts passed the specified design criterion (500 pulses at 20MW/m<sup>2</sup> with a hot coolant of 130°C) with a high degree of structural integrity.

Table 2. Summary of all HHF qualification test results.

| Test type  | Fatigue                  | Overload                           | Overload             |
|--|--------------------------|------------------------------------|----------------------|
| Applied heat flux  | 20MW/m <sup>2</sup>      | Screening                          | 25 MW/m <sup>2</sup> |
| Coolant temperature  | 130°C                    | 20°C                               | 20°C                 |
| Number of load cycles  | 500 pulses               | 5 pulses                           | 100 pulses           |
| W mono-block type (armour thickness: 8mm, block thickness: 12mm) |                          |                                    |                      |
| ITER-like (Cu layer: 0.1mm)                                      | no failure               | 32 MW/m <sup>2</sup>               | no failure           |
| ITER-like (Cu layer: 0.3mm)                                      | no failure               | 32 MW/m <sup>2</sup>               | no failure           |
| ITER-like (Cu layer: 1.0mm)                                      | no failure               | 32 MW/m <sup>2</sup>               | no failure           |
| Thermal break  | no failure               | 32 MW/m <sup>2</sup> <sup>3)</sup> | no failure           |
| W <sub>i</sub> /Cu composite pipe                                | no failure <sup>1)</sup> | 32 MW/m <sup>2</sup>               | no failure           |
| FGM interlayer (20μm)  | 82 pulses <sup>2)</sup>  |                                    |                      |
| FGM interlayer (0.5mm)   | no failure <sup>1)</sup> | 24 MW/m <sup>2</sup> <sup>4)</sup> |                      |
| W flat-tile type (armour thickness: 8mm, tile thickness: 12mm)   |                          |                                    |                      |
| W <sub>p</sub> /Cu composite block                               | 166 pulses               |                                    |                      |

1: 1000 pulses, 2: only 1 block, 3: surface melting, 4: JUDITH (e beam)

Furthermore, two design concepts (ITER-like, composite pipe) survived the overload HHF tests up to 32MW/m<sup>2</sup> in screening and up to 25MW/m<sup>2</sup> in cyclic loading (100-200 pulses). The thermal break type mock-up remained intact up to 30MW/m<sup>2</sup> in screening and 25MW/m<sup>2</sup> in cyclic loading (100 pulses).

The two different commercial grades of tungsten monoblocks (AT&M, ALMT) showed a comparably good performance in all HHF test modes. The ITER-like mock-ups with a thin Cu interlayer (0.1mm or 0.3mm) survived the fatigue test as well as the overload test. However, these mock-ups showed visible damage features at the Cu interlayer/CuCrZr pipe interface. Based on these results, the ITER-like target design (together with the HRP technology) was confirmed as baseline eligible for the conceptual design phase. In addition, the composite pipe target design was endorsed for further technology R&D (e.g. medium-scale production, radiation-resistant brazing).

## Acknowledgment

This work has been carried out within the framework of the EUROfusion Consortium and has received funding from the Euratom research and training program 2014-2018 and 2019-2020 under grant agreement No 633053. The views and opinions expressed herein do not necessarily reflect those of the European Commission.

## Data availability

The raw/processed data required to reproduce these findings cannot be shared at this time as the data also forms part of an ongoing study.

## References

- [1] M. Turnyanskiy, et al., Fus. Eng. Des. 96-97 (2015) 361-364.
- [2] R.A. Pitts et al., Nucl. Mater. Ener. 20 (2019) 100696.
- [3] N. Asakura et al., Fus. Eng. Des. 136 (2018) 1214-1220.
- [4] F. Maviglia, et al., Fus. Eng. Des. 109-111 (2016) 1067-1071.
- [5] C. Bachmann, Plant Description Document, EUROfusion report: 2KVVWQZ, 2020.
- [6] Th. Loewenhoff, et al., Phys. Scri. T145 (2011) 014057.
- [7] J.H. You, et al., Nucl. Mater. Ener. 23 (2020) 100745.
- [8] S. Noce, et al., Fus. Eng. Des. 155 (2020) 111730.
- [9] W. Timmis, Material assessment on the use of copper alloys in DEMO, EFDA Report WP12-MAT02-M03, 2013.
- [10] F.W. Wiffen, et al., Fusion materials research at ORNL in fiscal year 2018, ORNL/TM-2018/1072, 2018.
- [11] J.H. You, Nucl. Fusion 55 (2015) 113026 (11pp).
- [12] F. Crescenzi, et al, Fus. Des. Eng. 124 (2017) 432-436.
- [13] M. Li, et al., Fus. Des. Eng. 113 (2016) 162-170.
- [14] J.H. You, et al., Fus. Eng. Des. 124 (2017) 364-370.
- [15] G. Federici, et al., Fus. Eng. Des. 109-111 (2016) 1464-1474.
- [16] J.H. You, et al. Nucl. Mater. Ener. 16 (2018) 1-11.
- [17] J.H. You, et al., Nucl. Mater. Ener. 9 (2016) 171-176.
- [18] M Li, et al., Fus. Eng. Des. 124 (2017) 468-472.
- [19] M. Li, et al., Nucl. Mater. Ener. 14 (2018) 1-7.
- [20] F. Dompail, et al., Fus. Eng. Des. 154 (2020) 111497.
- [21] K. Zhang, et al., Fus. Eng. Des. 154 (2020) 111510.

- [22] E. Visca, et al., Fus. Eng. Des. 136 (2018) 1593-1596.
- [23] A. Lukenskas, et al., Fus. Eng. Des. 146 (2019) 1657-1660.
- [24] M. Richou, et al., Fus. Eng. Des. 157 (2020) 111610.
- [25] A. v. Müller, et al., Phys. Scr. T171 (2020) 014015 (8pp).
- [26] J.H. You, et al., J. Nucl. Mater. 305 (2002) 14-20.
- [27] A. v. Müller, et al., Nucl. Mater. Ener. 16 (2018) 163-167.
- [28] S. Fabritsiev, et al., Plasma Dev. Oper. 5 (1997) 133-141.
- [29] M. Fursdon, et al., Fus. Eng. Des. 160 (2020) 111831.
- [30] J.H. You, et al., J. Nucl. Mater. 438 (2013) 1-6.
- [31] E. Tejado, et al., Mater. Sci. Eng. A 712 (2018) 738-746.
- [32] E. Tejado, et al., J. Nucl. Mater. 498 (2018) 468-475.
- [33] H. Greuner, et al., Fus. Eng. Des. 146 (2019) 216-219.
- [34] H. Greuner, et al., Phys. Scri. T171 (2020) 014003 (7pp).
- [35] K. Zhang, et al., Fus. Eng. Des. 154 (2020) 111510.
- [36] J. H. You, et al., J. Nucl. Mater. 299 (2001) 1-8.
- [37] G. Dose, et al., Fus. Eng. Des. 146 (2019) 870-873.
- [38] J. H. You, Fus. Eng. Des. 38 (1998) 331-342.
- [39] J. H. You, et al., J. Nucl. Mater. 299 (2001) 1-8.
- [40] S. Roccella, et al., Fus. Eng. Des. 160 (2020) 111886.
- [41] M. Li, et al., Fus. Eng. Des. 122 (2017) 124-130.
- [42] H. Greuner, et al., J. Nucl. Mater. 367-370 (2007) 1444-1448.
- [43] M. Merola et al., Fus. Eng. Des. 85 (2010) 2312-2322.
- [44] G. Pintsuk, et al., Fus. Eng. Des. 88 (2013) 1858-1861.
- [45] M Li, et al., Fus. Eng. Des. 101 (2015) 1-8.
- [46] J.H. You, et al., Eurofusion report, in preparation.
- [47] W. Jacob, T. Schwarz-Sellinger, private communication.
- [48] M. Li, et al., Fus. Eng. Des. 90 (2015) 88-96.
- [49] M Li, et al., Fus. Eng. Des. 102 (2016) 50-58.
- [50] F. Maviglia, et al., Fus. Eng. Des. 109-111 (2016) 1067-1071.